Radiation hardness of high-Q silicon nitride microresonators for space compatible integrated optics

Victor Brasch,[1] Qun-Feng Chen,[2] Stephan Schiller[2] and Tobias J. Kippenberg[1,*]

[1]*École Polytechnique Fédérale de Lausanne, CH–1015, Switzerland*
[2]*Institut für Experimentalphysik, Heinrich-Heine-Universität Düsseldorf, DE–40225, Germany*

[*]*tobias.kippenberg@epfl.ch*

Abstract: Integrated optics has distinct advantages for applications in space because it integrates many elements onto a monolithic, robust chip. As the development of different building blocks for integrated optics advances, it is of interest to answer the important question of their resistance with respect to ionizing radiation. Here we investigate effects of proton radiation on high-Q ($\mathcal{O}(10^6)$) silicon nitride microresonators formed by a waveguide ring. We show that the irradiation with high-energy protons has no lasting effect on the linear optical losses of the microresonators.

OCIS codes: (130.3130) Integrated optics materials; (350.1820) Damage; (350.6090) Space optics; (230.5750) Resonators.

References and links

1. F. Berghmans, B. Brichard, A. Fernandez, A. Gusarov, M. Uffelen, and S. Girard.
2. M. T. Shetter and V. J. Abreu, "Radiation effects on the transmission of various optical glasses and epoxies," Appl. Optics **18**, 1132–1133 (1979).
3. T. P. Appourchaux, "Effect of space radiations on optical filters," Proc. SPIE **2018**, 80–91 (1993).
4. G. Naletto, A. Boscolo, J. Wyss, and A. Quaranta, "Effects of proton irradiation on glass filter substrates for the Rosetta mission," Appl. Optics **42**, 3970–3980 (2003).
5. Q.-F. Chen, A. Nevsky, S. Schiller, E. P. Campa, S. Lecomte, and D. Parker, "Proton irradiation robustness of dielectric mirrors for high-finesse Fabry-Pérot resonators in the near-infrared spectral range," Appl. Phys. B **116**, 1–7 (2013).
6. J. A. Wall and J. F. Bryant, "Radiation effects on fiber optics," Physical Sciences Research Papers (1975).
7. M. N. Ott, "Radiation effects data on commercially available optical fiber: database summary," Radiation Effects Data Workshop, 2002 IEEE pp. 24–31 (2002).
8. H. Henschel, O. Kohn, and U. Weinand, "Radiation hardening of pure silica optical fibres by high pressure hydrogen treatment," 6th European Conference on radiation and its effects on components and systems pp. 141–149 (2001).
9. M. Lezius, K. Predehl, W. Stower, A. Turler, M. Greiter, C. Hoeschen, P. Thirolf, W. Assmann, D. Habs, A. Prokofiev, C. Ekstrom, T. W. Hansch, and R. Holzwarth, "Radiation induced absorption in rare earth doped optical fibers," IEEE T. Nucl. Sci. **59**, 425–433 (2012).
10. H. Henschel, O. Koehn, and H. U. Schmidt, "Radiation-induced transmission loss of integrated optic waveguide devices," Proc. SPIE **1794**, 79–90 (1993).
11. V. Passaro and M. Armenise, "Neutron and gamma radiation effects in proton exchanged optical waveguides," Opt. Express **10**, 960–964 (2002).
12. S. Spaargaren and R. Syms, "Characterization of defects in waveguides formed by electron irradiation of silica-on-silicon," J. Lightwave Technol. **18**, 555–561 (2000).
13. W. Stutius and W. Streifer, "Silicon nitride films on silicon for optical waveguides," Appl. Optics **16**, 3218–3222 (1977).

#221160 - $15.00 USD Received 18 Aug 2014; revised 14 Oct 2014; accepted 19 Oct 2014; published 4 Dec 2014

14. D. J. Moss, R. Morandotti, A. L. Gaeta, and M. Lipson, "New CMOS-compatible platforms based on silicon nitride and Hydex for nonlinear optics," Nat. Photonics **7**, 597–607 (2013).
15. J. S. Levy, A. Gondarenko, M. A. Foster, A. C. Turner-foster, A. L. Gaeta, and M. Lipson, "CMOS-compatible multiple-wavelength oscillator for on-chip optical interconnects," Nat. Photonics **4**, 37–40 (2010).
16. T. Herr, K. Hartinger, J. Riemensberger, C. Wang, E. Gavartin, R. Holzwarth, M. L. Gorodetsky, and T. J. Kippenberg, "Universal formation dynamics and noise of Kerr-frequency combs in microresonators," Nat. Photonics **6**, 480–487 (2012).
17. T. Barwicz, M. Popović, P. Rakich, M. Watts, H. Haus, E. Ippen, and H. Smith, "Microring-resonator-based add-drop filters in SiN: fabrication and analysis." Opt. Express **12**, 1437–42 (2004).
18. F. Ferdous, H. Miao, D. E. Leaird, K. Srinivasan, J. Wang, L. Chen, L. T. Varghese, and A. M. Weiner, "Spectral line-by-line pulse shaping of on-chip microresonator frequency combs," Nat. Photonics **5**, 770–776 (2011).
19. S. Schiller, A. Görlitz, A. Nevsky, S. Alighanbari, S. Vasilyev, C. Abou-Jaoudeh, G. Mura, T. Franzen, U. Sterr, S. Falke, C. Lisdat, E. Rasel, A. Kulosa, S. Bize, J. Lodewyck, G. M. Tino, N. Poli, M. Schioppo, K. Bongs, Y. Singh, P. Gill, G. Barwood, Y. Ovchinnikov, J. Stuhler, W. Kaenders, C. Braxmaier, R. Holzwarth, A. Donati, S. Lecomte, D. Calonico, F. Levi, and m. o. t. S. Teams, "Towards neutral-atom space optical clocks (SOC2): Development of high-performance transportable and breadboard optical clocks and advanced subsystems," Let's embrace space **II**, 452–463 (2012).
20. S. Schiller, G. M. Tino, P. Gill, C. Salomon, U. Sterr, E. Peik, A. Nevsky, A. Görlitz, D. Svehla, G. Ferrari, N. Poli, L. Lusanna, H. Klein, H. Margolis, P. Lemonde, P. Laurent, G. Santarelli, A. Clairon, W. Ertmer, E. Rasel, J. Müller, L. Iorio, C. Lämmerzahl, H. Dittus, E. Gill, M. Rothacher, F. Flechner, U. Schreiber, V. Flambaum, W.-T. Ni, L. Liu, X. Chen, J. Chen, K. Gao, L. Cacciapuoti, R. Holzwarth, M. P. Heß, and W. Schäfer, "Einstein gravity explorer – a medium-class fundamental physics mission," Exp. Astron. **23**, 573–610 (2009).
21. B. Altschul, Q. G. Bailey, L. Blanchet, K. Bongs, P. Bouyer, L. Cacciapuoti, S. Capozziello, N. Gaaloul, D. Giulini, J. Hartwig, L. Iess, P. Jetzer, A. Landragin, E. Rasel, S. Reynaud, S. Schiller, C. Schubert, F. Sorrentino, U. Sterr, J. D. Tasson, G. M. Tino, P. Tuckey, and P. Wolf, "Quantum tests of the Einstein equivalence principle with the STE-QUEST space mission," arXiv **1404.4307** (2014).
22. J. F. Ziegler, "SRIM Software," http://www.srim.org (2013).
23. T. J. Kippenberg, S. M. Spillane, and K. J. Vahala, "Kerr-nonlinearity optical parametric oscillation in an ultrahigh-Q toroid microcavity," Phys. Rev. Lett. **93**, 83904 (2004).
24. J. Riemensberger, K. Hartinger, T. Herr, V. Brasch, R. Holzwarth, and T. J. Kippenberg, "Dispersion engineering of thick high-Q silicon nitride ring-resonators via atomic layer deposition," Opt. Express **20**, 27661–27669 (2012).
25. W. N. MacPherson, R. R. J. Maier, J. S. Barton, J. D. C. Jones, A. F. Fernandez, B. Brichard, F. Berghmans, J. C. Knight, P. S. Russell, and L. Farr, "Dispersion and refractive index measurement for Ge, B-Ge doped and photonic crystal fibre following irradiation at MGy levels," Meas. Sci. Technol. **15**, 1659 (2004).
26. P. Del'Haye, O. Arcizet, M. L. Gorodetsky, R. Holzwarth, and T. J. Kippenberg, "Frequency comb assisted diode laser spectroscopy for measurement of microcavity dispersion," Nat. Photonics **3**, 529–533 (2009).
27. M. L. Gorodetsky, A. D. Pryamikov, and V. S. Ilchenko, "Rayleigh scattering in high-Q microspheres," J. Opt. Soc. Am. B **17**, 1051–1057 (2000).
28. T. J. Kippenberg, S. M. Spillane, and K. J. Vahala, "Modal coupling in traveling-wave resonators," Opt. Lett. **27**, 1669–1671 (2002).
29. D. L. Griscom, M. E. Gingerich, and E. J. Friebele, "Radiation-induced defects in glasses: Origin of power-law dependence of concentration on dose," Phys. Rev. Lett. **71**, 1019–1022 (1993).
30. D. L. Griscom, "Trapped-electron centers in pure and doped glassy silica: A review and synthesis," J. Non-Cryst. Solids **357**, 1945–1962 (2011).
31. "ESA document 'STE-QUEST environmental specification'," issue 1 revision 0, reference js-10-12, May (2012).
32. F. Lei, P. R. Truscott, C. S. Dyer, B. Quaghebeur, D. Heynderickx, P. Nieminen, H. Evans, and E. Daly, "MULASSIS: a Geant4-based multilayered shielding simulation tool," IEEE T. Nucl. Sci. **49**, 2788–2793 (2002).
33. "MUlti-LAyered Shielding SImulation Software (MULASSIS)," http://reat.space.qinetiq.com/mulassis/ .

1. Introduction

Optics has been an important part of space systems ever since the early years of space exploration. While imaging optics were part of some of the first instruments in space, the field of optics keeps expanding and in particular the field of integrated optics shows great potential for multiple applications with its distinct advantages of small size, robustness against vibrations and high degree of integration. The effect of ionizing radiation in space has been tested in many studies for discrete optics [1–5] as well as fiber optics [1, 6–9]. From these studies it is well known that radiation can change the optical properties of glasses which can lead to increased losses. However, this important aspect of space compatibility has not

#221160 - $15.00 USD Received 18 Aug 2014; revised 14 Oct 2014; accepted 19 Oct 2014; published 4 Dec 2014

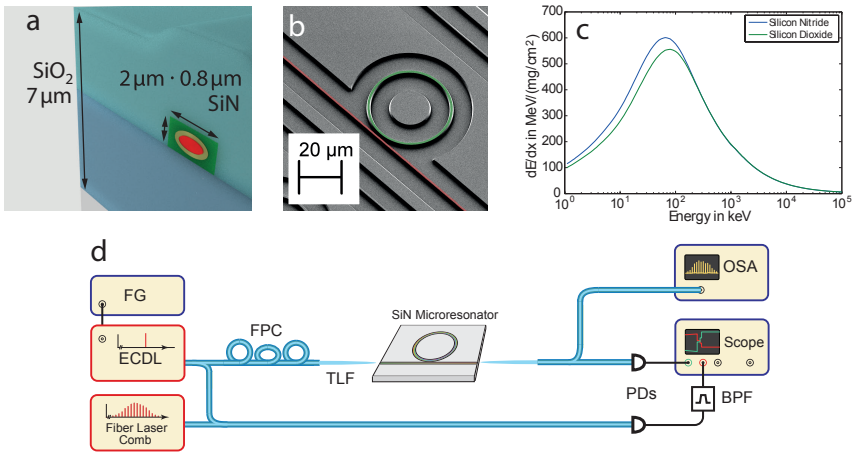

Fig. 1. (a) Schematic cross-section of the system tested. The silicon nitride waveguide is shown in green with an approximated intensity distribution for a fundamental mode around 1550 nm inside (red). The silicon dioxide cladding above and below differ slightly as they have been deposited or grown using different methods. (b) Colored electron microscopy image of a SiN microresonator (not one tested and with smaller radius) without the glass cladding. The resonator waveguide is colored green while the bus waveguide is colored red. (c) Energy loss function for protons with energies ranging from 1 keV to 100 MeV in silicon nitride and silicon dioxide calculated with SRIM [22]. (d) Schematic of the setup used for the characterization. ECDL: external cavity diode laser; FG: function generator for the sweep of the laser; FPC: fiber polarization controller; TLF: tapered lensed fibers to couple to the chip; PD: photo diodes; BPF: electrical band-pass filter; OSA: optical spectrum analyzer

been investigated extensively for integrated optics [10–12]. Here we study the radiation hardness of waveguide microresonators made from silicon nitride (SiN) [13, 14] with quality factors (Q-factors) around 10^6. These microresonators can find applications as optical frequency comb generators and optical filters [15–17]. The optical frequency combs generated inside the resonators have frequency spacings of around 10 GHz to 1 THz and span several hundred nm [15, 16, 18]. Frequency combs can be crucial parts of future space missions and applications. Examples for missions in the field of fundamental physics that would benefit of such a device are the missions "Space Optical Clock" (SOC) [19] on the ISS, the "Einstein Gravity Explorer" (EGE) [20], and the "Space Time Explorer and Quantum Test of the Equivalence Principle" (STE-QUEST) [5,21]. In the first and second mission, a frequency comb is required to convert the laser radiation of an optical clock into microwave radiation that is transmitted to ground where its frequency is measured. In the STE-QUEST mission, a microwave-optical local oscillator has been proposed as part of a microwave cold Cs atomic clock, which provides, again via conversion by a frequency comb, an ultra-stable 9 GHz microwave for interrogation of the atomic clock.

The generation of microresonator frequency combs relies on the Kerr nonlinearity of the silicon nitride resonator. The effect of the nonlinearity is greatly enhanced by the high Q-factor of the resonator, the threshold for the parametric oscillation scales as $1/Q^2$ [16, 23]. Therefore the Q-factor of a microresonator is an important parameter for these applications. It depends on the intrinsic optical losses due to absorption and scattering as well as the coupling losses to the bus waveguide that is used to couple light to the resonator. Assuming that the coupling losses

#221160 - $15.00 USD Received 18 Aug 2014; revised 14 Oct 2014; accepted 19 Oct 2014; published 4 Dec 2014

are constant, a change in Q-factor directly relates to changed losses of the waveguide of the resonator.

One of the key requirements for space equipment is radiation resistance. Satellites on orbits that cross the Van Allen belt are exposed strongly to electron and proton radiation. Components of instruments that are to be flown on such orbits must therefore be tested beforehand with respect to their radiation resistance. The mentioned missions EGE and STE-QUEST rely on such orbits. In this work, we perform a first investigation of the influence of proton radiation on the Q-factor as a key property of microresonators.

2. Microresonator design and measurement procedure

The microresonators under test are waveguide ring resonators. A silicon nitride (SiN) waveguide with dimensions 0.8 μm by 2 μm and with a refractive index of 1.98 confines the light and is embedded into a silicon dioxide (SiO_2) cladding with refractive index of approximately 1.45 (Fig. 1(a)). From simulations we know that at 1550 nm about 80 % of the power travels inside the SiN and 20 % in the SiO_2. To fabricate the ring microresonators, standard (p-doped boron doping, resistivity of 10 to 20 Ωcm for Wafer 2) 100 mm silicon wafers are oxidized in a thermal wet oxidation process in order to grow a film of 6 μm (Wafer 1) and 4 μm (Wafer 2) SiO_2. On top, 800 nm of silicon nitride (Si_3N_4) is deposited as nearly stoichiometric high-stress thin film via low pressure chemical vapor deposition (LPCVD). After patterning the silicon nitride using electron-beam lithography and reactive-ion etching both wafers are annealed for a first time and Wafer 2 undergoes a deposition step to obtain a 30 nm thin layer of hafnium dioxide on top of the waveguide [24]. Afterwards the 3 μm thick SiO_2 top cladding is deposited as low-temperature CVD oxide on both wafers followed by a second thermal anneal. In a last step chips of 5 mm by 5.5 mm are separated. One chip comprises multiple resonators of the same size. Each resonator is evanescently coupled to one separate bus waveguide which allows to couple light in and out of the resonator (Fig. 1(b)). Further details about the fabrication process can be found in [24].

As outlined above, the Q-factor is one of the most important properties of the resonator and the most likely to undergo significant changes under irradiation [7, 25]. Therefore we selected one chip from each of the two wafers (Chip 1 from Wafer 1 with a free spectral range (FSR) of around 75 GHz , Chip 2 from Wafer 2 with an FSR of around 45 GHz) which were fabricated in different runs approximately four months apart. For two resonators on each chip we characterized their Q-factors. The quality factor was measured by determining the loaded linewidth ($\kappa/2\pi$ in Hz) of resonances between 1520 and 1580 nm of the respective resonator. The Q-factor relates to the linewidth as $Q = \omega/\kappa$ where ω is the optical resonance frequency. The linewidths of the resonances were measured by coupling an external cavity diode laser via the bus waveguide to the resonator. Scanning the laser in frequency over the resonance frequency of the respective resonance results in a typically Lorentzian shaped dip in the transmitted laser power which is recorded over the scan time (Fig. 1(d)). The linewidth of the laser is approximately 300 kHz, much narrower than the measured resonances. Examples of the resulting power over time traces of such scans are show in Fig. 2. Each individual laser scan only lasts for tens of ms and long term effects such as the drift of the laser or slow power variation can be neglected. Additionally the scan span is very small (of the order of 2 GHz) such that the output power can be considered to be constant during the scan. The polarization does not have an effect on the linewidths of the resonances, however, the contrast and the lineshape depend on the polarization. Therefore the polarization of the laser was optimized by hand to yield minimal transmission through the bus waveguide with the laser on resonance and a lineshape with as little deviation from a Lorentzian shape as possible. The laser scan was calibrated in frequency using a fiber frequency comb which provides a frequency calibration marker approximately ev-

#221160 - $15.00 USD Received 18 Aug 2014; revised 14 Oct 2014; accepted 19 Oct 2014; published 4 Dec 2014

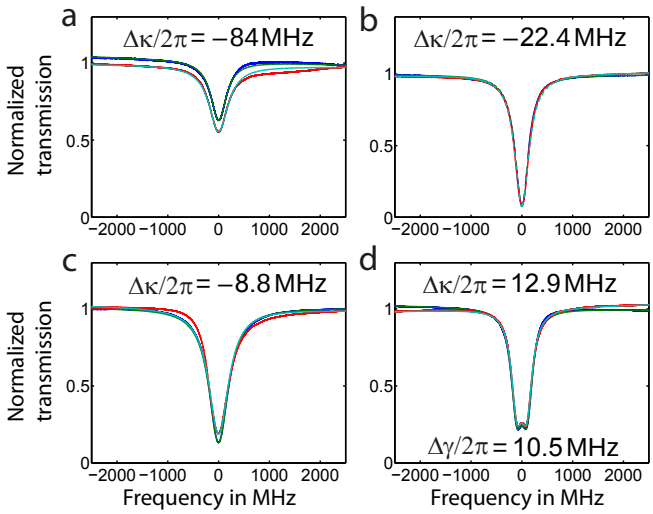

Fig. 2. Four measurements of total linewidths and their fits from resonator III. Dark blue is the measurement before radiation, red the measurement after radiation. Green and light blue are the fits for pre and post radiation respectively. $\Delta\kappa/2\pi$ is the difference in fitted resonance widths as plotted in Fig. 4. $\Delta\gamma/2\pi$ is the difference in the fitted splitting of the resonance in the two fits. These differences are caused by the polarization dependency of the exact lineshape of the resonance.

ery 120 MHz with 1 MHz precision [24, 26]. In most cases a good fit of the transmission curve could be obtained with a simple Lorentzian lineshape function. For resonances that showed a splitting due to the coupling of the co- and counter-propagating modes, we fitted a model that takes this splitting into account [27,28]. The average linewidths of the four measured resonators (resonator I to IV) varied from 250 MHz to 440 MHz. In total we charaterized 311 resonances. By determining the exact relative positions of many resonances we are also able to measure the FSR of the fundamental mode families of the resonators. As the FSR is related to the effective refractive index n_{eff} of the mode inside the resonator as $FSR = \frac{c}{2\pi r n_{\text{eff}}}$ where r is the radius of the ring resonator, a change in the refractive indices of the materials (either the SiN of the core or the SiO_2 of the cladding) should be visible as a change in the FSR of the modes.

After the initial characterization the chips were sent for the irradiation. After the irradiation was performed as described below the chips were shipped back and the linewidths were measured again to check for changes. For each resonance that was measured before the irradiation the polarization-dependent shape of the resonance was again optimized to yield a minimal transmission on resonance (for resonances of Chip 1 from Wafer 1 with resonators I and II) or to obtain a best possible match with the shape of the resonance measured before the irradiation (Chip 2 from Wafer 2 with resonator III and IV). Due to the shipments and the preparation for the irradiation as well as the extensive manual measurements the whole procedure stretched over 12 weeks. Therefore, potentially short lasting irradiation effects as they have been reported in fibers [9, 29] are not well reflected in our measurements.

3. Space proton irradiation spectrum

Proton irradiation of the sample can have multiple effects which are caused by the interaction with the material [1]. The effect that is usually considered to be the most important for radiation

#221160 - $15.00 USD Received 18 Aug 2014; revised 14 Oct 2014; accepted 19 Oct 2014; published 4 Dec 2014

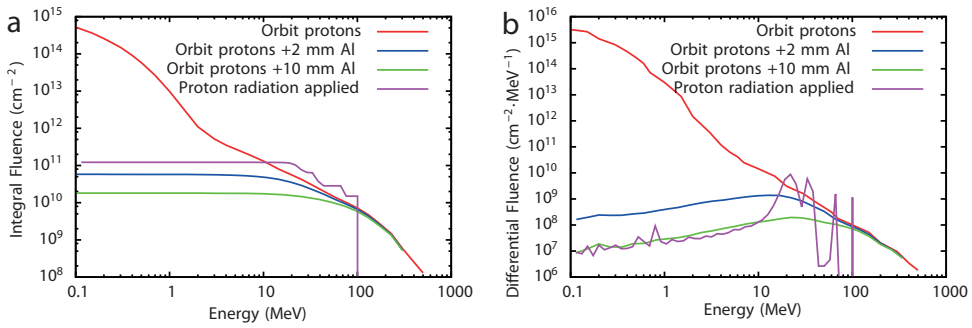

Fig. 3. (a) Red, time-integrated and energy-integrated (integral) proton fluence expected during the 5-year-long STE-QUEST mission; blue, same, but behind a 2 mm thick aluminum shield; green, same, but behind a 10 mm thick aluminum shield; purple, integral fluence of the proton radiation applied in the test. (b) The corresponding time-integrated differential fluences. The bin width at $E = 99.7$ MeV in the plot (b) is 13 MeV. "Orbit protons" refers to the proton spectrum on the STE-QUEST orbit, with duration of 5 years. "Proton radiation applied" is the radiation impinging onto the tested microresonators.

induced optical absorption in silicon dioxide based materials is the formation of color centers [6, 9, 30]. As the critical part of our chips is only around 8 μm thick, most of the protons with energies above approximately 1 MeV pass through this part. The average energy deposited in the sample depends on the energy loss function as it can be calculated for different materials. In Fig. 1(c) the results of simulations for the two relevant materials for this work, silicon nitride and silicon dioxide, are shown.

The starting point of the irradiation study is the result of modeling the proton spectrum experienced by a spacecraft on a specific orbit. We assume here the highly elliptic orbit proposed for the STE-QUEST mission. It is characterized by a 16-hour period, a perigee altitude (above ground) varying between 800 and 2400 km during the course of the 5-year long mission, and a constant apogee altitude of approximately 51 000 km [21]. The time-averaged spectral (i.e. energy-dependent or differential) fluence of the proton radiation, and the corresponding time-averaged and energy-integrated (integral) fluence of the protons, calculated in [31], are shown in Fig. 3 (red line). The energy-integrated fluence at energy E is defined as the integral of the differential fluence from infinite energy down to E. Note that the two quantities have a similar energy dependence for this orbit. The quantities refer to the radiation arriving on the satellite.

When one considers the radiation reaching a particular component in an instrument in the satellite, one must consider that this component is shielded by other components of the satellite (satellite structure, solar panels, housing of the instrument, additional specific shielding layers) in a way that depends on the details of the spacecraft and the instruments. The amount of shielding can be different in different directions with respect to the spacecraft axes. The details are usually not known with certainty a priori, since they are worked out during the detailed planning of the mission, which only occurs after selection of the mission by the space agency.

We therefore first consider as an example a shielding having an equivalent thickness of 2 mm aluminum (blue lines in Fig. 3). Such a thickness is likely to be present even without installing additional shielding. We see that the result is an extremely strong reduction of the fluences at energies below 10 MeV. The modified fluence was computed using the software MULASSIS [32, 33]. In this program, one layer of aluminum shielding is considered and the modification of an input spectrum is then calculated, yielding an output spectrum.

#221160 - $15.00 USD Received 18 Aug 2014; revised 14 Oct 2014; accepted 19 Oct 2014; published 4 Dec 2014

We can assume the existence of 10 mm aluminum shielding, which would arise from structural shielding plus possibly an additional custom housing enclosing the microresonator. The resulting fluences reaching the component are shown in green in the plots. The increased shielding thickness results in an additional factor 10 reduction in the fluences below 10 MeV. The fluences then have values that are well accessible by an irradiation run produced by a proton accelerator. The task is then to devise an irradiation protocol that models the predicted, shielded space proton spectrum reasonably well.

4. Irradiation protocol

The proton irradiation test was carried out at the Paul Scherrer Institut (PSI) in Villigen, Switzerland. The maximum energy available at this facility is 99.7 MeV. This sets an upper limit for the energy of the space proton spectrum that can be reproduced. Considering that protons with energy lower than 20 MeV would be effectively stopped (i.e. absorbed) by a 2 mm aluminum shield, the samples were irradiated with protons with energies on the order of and higher than 20 MeV. The samples were irradiated with 4 energies, 18.3, 30.7, 61.6, and 99.7 MeV. Except for the last one, these energies are the mean energies after degradation of the proton beam by a copper plate ("degrader") of thickness 12.5, 11.5, and 7.5 mm, respectively, inserted into the proton beam. The fluences of the proton beam (upstream of the respective degrader) were set to 6.000×10^{10}, 4.003×10^{10}, 1.416×10^{10}, and 1.516×10^{10} protons/cm^2, respectively .

The integral and differential fluence of the implemented irradiation of the samples are shown in purple in Fig. 3. They are the sum of four individual fluences, each of which corresponds to the simulated fluence of a 99.7 MeV proton beam degraded by the respective copper degrader (if any).

In more detail, the differential fluence reproduces well the low-energy region ($E < 10$ MeV) of the 10 mm shielded space spectrum. In the range 18 to 100 MeV the spectrum consists of four peaks, rather than a continuous spectrum, which are remainders of the energies of the proton beam. We believe that this is of no consequence; in other words, the potential damage done to the sample will likely not depend on the details of the energy spectrum in the range $18 - 100$ MeV. The overall situation is that the implemented integral fluence exceeds both the 10 mm-shielded as well as the 2 mm-shielded integral space fluence at all energies $E < 100$ MeV. Therefore, the implemented fluence is a conservative choice for a 5-year STE-QUEST mission duration having a 10 mm aluminum shielding. In addition, the integral fluence down to $E = 18$ MeV is a factor 2 above the unshielded STE-QUEST space spectrum (red line in the figure), also indicating the conservative nature of our test irradiation protocol.

5. Results

In Fig. 4 the mean linewidths of pre and post radiated samples $(\kappa_{\text{after}} + \kappa_{\text{before}})/4\pi$ as well as the difference in linewidths ($\Delta\kappa/2\pi = \kappa_{\text{after}}/2\pi - \kappa_{\text{before}}/2\pi$) between the measurements are shown. To determine the possible effects of the radiation on the Q-factor $\Delta\kappa$ is plotted in histograms and fitted for each resonator independently with a Gaussian distribution ($P(\Delta\kappa) = A \times e^{-(\Delta\kappa - \langle\Delta\kappa_f\rangle)^2/2\sigma^2}$) in order to localize the center ($\langle\Delta\kappa_f\rangle$) as shown in Fig. 4 (b). The fits show that the deviation of the center from 0 is of the order of 1 % of the linewidth. For two of the fits (green and red) the 0 is within the 95% confidence interval of the fit for one (dark blue) the full confidence interval is below 0 and for the last (light blue) it is above 0. This shows that there is no significant lasting effect of the radiation dose used. The widths of the distributions from the fits vary between 10 and 20 MHz. This spread of the distribution is caused by the dependency of the exact shape of the resonance on the polarization and interference effects which cause distortions of the lineshape. Examples of data and fits are shown in Fig. 2. The measurements in Fig. 2(a) look very similar but show a significant deviation in the result of the

#221160 - $15.00 USD Received 18 Aug 2014; revised 14 Oct 2014; accepted 19 Oct 2014; published 4 Dec 2014

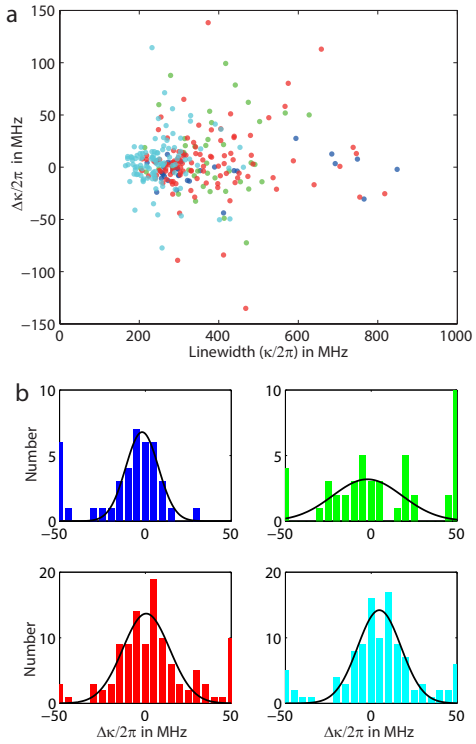

Fig. 4. (a) Change in total linewidth ($\Delta\kappa/2\pi$=$\kappa_{\text{after}}/2\pi - \kappa_{\text{before}}/2\pi$) of the resonances of four resonators (dark blue, green, red, light blue) plotted over averaged linewidth $(\kappa_{\text{after}} + \kappa_{\text{before}})/4\pi$. Average linewidths for one resonator are 370, 440, 380 and 250 MHz for resonator I (dark blue) and II (green) on Chip 1, III (red) and IV (light blue) from Chip 2 respectively. (b) histograms of the change in linewidth for each resonator, same dataset with same colors as in (a). The black lines represent the fitted Gaussian distributions. The outermost bins of the histograms on either side have been excluded for the fits. The values obtained for the mean of the distribution as offset from 0 ($\langle\Delta\kappa_f\rangle/2\pi$) are -1.9, -2.2, 0.5 and 4.7 MHz for resonator I, II, III and IV respectively. The standard deviation in the same order are 9.5, 20.3, 13.7 and 12.6 MHz.

fit. Although the other measurements shown almost fall on top of each other for large parts, the fitted linewidths still deviate by some MHz. The measurement in Fig. 2(d) shows a split resonance which is fitted with an appropriate function as described above.

Furthermore the good agreement of the shape of the resonances before and after radiation shows that the ratio of waveguide losses to coupling losses did not change significantly. A change of this ratio would change the depth of the resonance. One potential reason for changes in the coupling losses could be changes of the refractive index of the materials. As described above this would affect the free spectral range of the resonators. Comparing the measured FSR before and after the irradiation shows that the deviation is smaller than 1% for all measured modes. This is within the precision of our measurement technique and indicates that the refractive indices of the materials do not change significantly. Similarly the absolute position of the resonances as measured with an optical spectrum analyzer did not change by more than the measurement imprecision (approximately 0.1 nm) which also supports the conclusion that the refractive indices of the materials did not change.

#221160 - $15.00 USD Received 18 Aug 2014; revised 14 Oct 2014; accepted 19 Oct 2014; published 4 Dec 2014

Comparing the results with other radiation experiments is not easy because of different radiation types, radiation energies and fluences as well as differences in the wavelength of the light that the optical losses are measured for. In particular there is only very little work describing the effect of radiation on integrated waveguide structures. As our structures are made of silicon nitride and silicon dioxide, a comparison with a non-doped standard optical fiber might be the most appropriate. For the particular case of SMF28 fiber measured at around 1550 nm it has been shown that a change of the transmission losses can be observed for irradiation with protons with 280 MeV energy, much above the energies used in this study but with a similar fluence. For lower energies (20 MeV) the transmission did not change [9].

In conclusion we have shown that high-energy proton radiation does not lead to a lasting degradation of silicon nitride microresonators for Q-factors of the order of 10^6. Although short term effects directly after the irradiation [9] could have remained undetected, we show conclusively that there are no long term, lasting effects. Moreover the refractive index of the materials did not change significantly. These results can also be applied to silicon nitride waveguides with a structure similar to the ones measured here.

Our work therefore paves the way for the rather young platform of silicon nitride waveguides towards more integrated and robust devices in space applications. Such devices can be microresonator-based optical frequency combs.

Acknowledgments

We thank H. Luckmann and A. Nevsky for assistance and the PSI Villigen for the irradiation. This work was partially supported by the European Space Agency (ESA), the DARPA QuASAR program, by the Bundesministerium für Wirtschaft und Technologie (Germany) under project no. 50OY1201 and by the Swiss National Science Foundation (SNF).